An Overview of Equivalent Circuit Modeling Techniques of Frequency Selective Surfaces and Metasurfaces

Filippo Costa, Agostino Monorchio, and Giuliano Manara

Dipartimento di Ingegneria dell'Informazione
University of Pisa, Pisa, 56122, Italy
filippo.costa@iet.unipi.it, a.monorchio@iet.unipi.it, g.manara@iet.unipi.it

Abstract ─ Circuit analysis of frequency selective surfaces is reviewed with the aim to underline range of validity of different models and their advantages in terms of simplicity and physical insight. The circuit approach is based on an equivalent representation of the FSSs with series or shunt connections of inductances and capacitances. Dense non-resonant periodic surfaces (i.e.: grid or patch arrays) can be analyzed analytically by computing the values of inductors or capacitors via the homogenization theory. As the lattice period increases with respect to the operating wavelength or the element shape becomes resonant, a fully analytical circuital approach fails, in particular, in the presence of thin substrates. However, simple circuit approaches can still be employed by deriving lumped parameters values via a quick pre-processing and then generalizing them. The results are accurate up to the resonant frequency region of the element. By including an additional lumped element it is possible, taking into account the effect of the first high order Floquet harmonic. The multi-mode formulation is also able to catch the highly non-linear response of FSS screens in the grating lobe region provided that the current profile of the element does not change significantly.

Index Terms ─ Equivalent circuit model, frequency selective surfaces, periodic gratings.

I. INTRODUCTION

The fact that non-continuous surfaces can diffract electromagnetic waves, was proved for the first time by the American physicist David Rittenhouse in 1786 [1]. He found explanation to the curious phenomenon observed by Mr. Hopkinson, that is, the presence of multiple images when he tried to observe a distant street lamp through a silk handkerchief. Rittenhouse reproduced a grating by using 50 hairs between two finely threaded screws. In 1821, Fraunhofer built a similar diffraction grating which used to measure wavelength of specific colors and dark lines in the solar spectrum [2]. In 1902 and 1904, Wood [3] and Rayleigh [4] debated on the popular Wood's anomalies of periodic gratings. Rayleigh formulated a theory that was able to predict diffraction angles of the grating [5], but a comprehensive understanding of resonance effects observed by Wood was achieved with the papers of Fano in 1941 [5], and Hessel and Oliner in 1965 [7]. Probably, the first microwave application of gratings at microwaves by Marconi and Franklin who designed in 1919 a parabolic reflector built of wire sections instead of a continuous surface [8]. Although, the concept of frequency selective surface is known at microwaves since the beginning of 20th century, the filtering capability of these periodic surfaces were scarcely exploited. Some applicative works have been done in the fifties: in 1956, Trentini proposed the use of gratings for enhancing the gain of antennas [9]. In the same period, Marcuvitz, Oliner and other scientists studied the properties of waveguides loaded with periodic structures [10]-[12] and proposed waveguide antennas based on leaky-waves [13]-[16]. Besides the aforementioned seminal research findings, early practical applications of selective surfaces were mainly focused in Cassegainian subreflectors in parabolic dish antennas. The satellite Voyager 77 exploited a frequency selective surface for implementing a double-frequency reflector [17]. The principle was

Submitted On: March 1, 2014
Accepted On: July 25, 2014

extended to four frequency bands in the satellite Cassini in 1996 [18]. Nowadays, FSSs [19], [20] are employed at microwave frequencies for designing frequency selective radomes [21], leaky wave/Fabry-Perot, low-profile and low-RCS antennas [22]-[24], reflectarays, trasmittarrays and lenses [25], [26], polarization converting surfaces [27], waveguide filters [28], electromagnetic shielding [29], radar absorbing materials [30], and more in general, to synthesize the bidimensional version of metamaterials, that is, metasurfaces [31]. In the THz domain, Frequency Selective Surfaces are frequently addressed as metasurfaces and are massively employed for designing sensors, spatial filters, absorbers, THz modulators and imaging devices [32]-[34]. In optical domain, FSSs have been recently proposed to improve the efficiency of photovoltaic cells [35], [36], but more frequently they are employed to achieve light diffraction (diffraction gratings). In the latter case, the lattice period is several wavelengths for achieving light diffraction towards different directions. Diffraction gratings are used in several optical commercial devices such as monochromators, spectrometers, lasers, wavelength division multiplexing devices, optical pulse compressing devices, optical microscopes and many others [2].

Classical numerical methods for the analysis of frequency selective surfaces are based on the Finite Difference Time Domain (FDTD) or Finite Element Method (FEM) techniques. These methodologies can be applied to arbitrary FSS configurations (single-layer, multi-layer, finite, and curved frequency-selective surfaces), but they are computationally onerous. Conversely, other dedicated highly efficient methods have been proposed since the seventies. The most famous is the Integral Equation Method (IEM), used in conjunction with the Method of Moments (MoM) [37]-[40].

A helpful way to understand the FSS behavior is to establish an analogy between lumped filters and the periodic surfaces. A circuital analysis, unlike full-wave simulations, provides immediate results and a good physical insight into the design properties of the structure.

This paper is organized as follows. In the next section a comprehensive review of the literature is presented. The third section is dedicated to the description of three efficient methods to represent the FSS response in different operating regimes. In the fourth section it describes a simple procedure for calculating the transmission and reflection coefficient of the FSS within a multi-layer. Lastly, the fifth section describes the results obtained with the equivalent circuit models on various meaningful examples of FSS elements.

II. LITERATURE REVIEW OF FSS MODELLING

In the beginning of 20th century, MacFarlane [41], Wessel [42], and Hornejäger [43] showed that the scattering problem of a parallel wire grid can be solved using a transmission line model, where the wire grid is modeled as a shunt impedance and the homogeneous surrounding medium is modeled as infinite transmission lines. Initially, only simple elements comprising wire grids or patches were considered. Later, Trentini [44] included the periodical loading of the wire grid with lumped circuit elements, and Wait developed the MacFarlane model to analyze the reflection properties in the vicinity of a dielectric interface [45], [46]. In the sixties, Ulrich [47] improved the equivalent circuits for inductive and capacitive grids with an additional capacitor or inductor, respectively, to take into account resonant effects of these structures as the periodicity of the mesh becomes approximately equal to λ. The value of these extra circuit elements was evaluated from the measurements by matching the resonance at in the circuit model with measurements. Lee and Zarrillo [48] compared the accuracy of different models for inductive or capacitive grids.

An alternative way to derive the impedance of the metallic grids was proposed by Kontorovich and Astrakhan in [49], [50] by averaging the currents flowing on the periodic structure. The expression of the surface impedance for array of patches can be obtained by using the Babinet principle [51]. The averaged model works properly in the quasi-static regime where grids or patches have respectively a pure inductive and capacitive behavior. When the frequency increases up to the first resonance, this model clearly fails because it does not take into account any resonance phenomenon. The accuracy of the averaged capacitances/inductances can be improved further by taking into account terms of higher orders [52]. The main limitations of these

models are:

- *only simple FSS configurations are considered;*
- *the effect of a thin nearby material interface is not adequately modeled.*

Attempts to derive formulas for more complex FSS shapes (e.g., loops, crosses, Jerusalem crosses) have been made in the eighties [53]-[57], but the derived formulas often contain empirical derived correction factors turning out to lose the intuitive understanding on which a model is based.

The effect of substrates is generally taken into account by multiplying the FSS capacitance through the averaged permittivity of the dielectrics enclosing the FSS [51]. This approximation is acceptable only for thick dielectric substrates (thicker than an half of the cell periodicity) or when the FSS periodicity is much lower than the operating wavelength [58], [59]. In practical cases, the supporting dielectrics are usually much thinner than the wavelength, and the dielectric thickness also has to be taken into account in computing the averaged permittivity. In order to achieve more accurate results, valid also for thin substrates, a corrected single mode circuit [58] or a multi-mode formulation may be adopted [60]-[62].

III. FSS MODELING

An important parameter in the FSS analysis is the wavelength at which the grating lobes or trapped modes onset [1], [63]. For freestanding FSS, the wavelength of the first high order Floquet harmonic reads:

$$\lambda_g^{\varepsilon_r} = D\left(\sqrt{\varepsilon_r} + \sin\left(\vartheta\right)\right), \qquad (1)$$

where D represents the inter-element spacing, c is the speed of light and θ is the incident angle, and ε_r is the dielectric permittivity of the media where the FSS is embedded. For wavelengths longer that λ_g (or frequencies smaller that c/λ_g) the only propagating Floquet harmonic is the fundamental one. Higher modes are evanescent and decay exponentially away from the mesh. At normal incidence, the grating lobes wavelength is equal to the FSS periodicity. However, it has to be pointed out that when the FSS is embedded with dielectric media, the first high-order phenomenon is represented by the onset of trapped dielectric modes [19] (or trapped surface waves) that occurs well below the propagation of the first grating lobe.

In the analysis of periodic structures, three different fundamental regions can be individuated [63]. At long wavelengths, when the FSS periodicity D is much larger than the operating wavelength λ, quasi-static regime, the periodic surface can be efficiently analyzed by using homogenized theory. The intermediate frequency range, where the FSS periodicity is smaller but comparable with the operating wavelength, the periodic surface element can be resonant. In this region the FSS can still be modeled by using the circuit theory, but the values of the lumped parameters need to be retrieved by using full-wave simulations followed by an inversion procedure. The last region, where the operating wavelength becomes shorter than guided wavelength λg, is highly non-linear because more than one Floquet harmonic is in propagation and FSS elements (also single resonant ones) need to be represented by using a multi-mode network. The three regions are summarized in Fig. 1. In the following paragraphs we briefly summarize three efficient approaches for analyzing FSSs in the three described frequency regions.

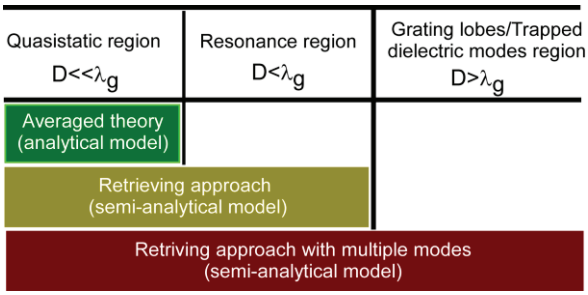

Fig. 1. Three characteristic regions of periodic structures.

A. Averaged approach

For simple non-resonant elements as wire grids or patch arrays, the impedance is mainly inductive or capacitive, respectively [65] (Fig. 2). The calculation of the inductance or the capacitance value can be accomplished by averaging the currents flowing on the periodic structure. The derived FSS impedance is of the second order since it is angle dependent and it has a different expression for the TE and the TM polarization. In the case of a patch array, the impedance $Z_{patch}^{TE/TM} = 1/\left(j\omega C_{patch}\right)$, is just a capacitor [51]:

$$C_{patch}^{TE} = \frac{D\varepsilon_0\left(\varepsilon_{r1}+\varepsilon_{r2}\right)}{\pi}\ln\left(\frac{1}{\sin\left(\frac{\pi w}{2D}\right)}\right)\left(1-\frac{k_0^2}{k_{eff}^2}\frac{\sin^2\left(\vartheta\right)}{2}\right)$$

$$C_{patch}^{TM} = \frac{D\varepsilon_0\left(\varepsilon_{r1}+\varepsilon_{r2}\right)}{\pi}\ln\left(\frac{1}{\sin\left(\frac{\pi w}{2D}\right)}\right), \quad (2)$$

while for grids, the impedance $Z_{grid}^{TE/TM} = j\omega L_{grid}$, is an inductor:

$$L_{grid}^{TE} = \frac{D\mu_0}{2\pi}\ln\left(\frac{1}{\sin\left(\frac{\pi w}{2D}\right)}\right)$$

$$L_{grid}^{TM} = \frac{D\mu_0}{2\pi}\ln\left(\frac{1}{\sin\left(\frac{\pi w}{2D}\right)}\right)\left(1-\frac{k_0^2}{k_{eff}^2}\frac{\sin^2\left(\vartheta\right)}{2}\right), \quad (3)$$

where D represents the periodicity of the FSS, w is the gap between the squares patches and k_0 is the wave number in free space, $k_{eff} = k_0\sqrt{\left(\varepsilon_{r1}+\varepsilon_{r2}\right)/2}$ is the wave number of the incident wave vector in the effective host medium, θ is the incident angle. ε_{r1} and ε_{r2} are the relative dielectric permittivity of the dielectric slabs surrounding the periodic surface (typically the upper dielectric is air).

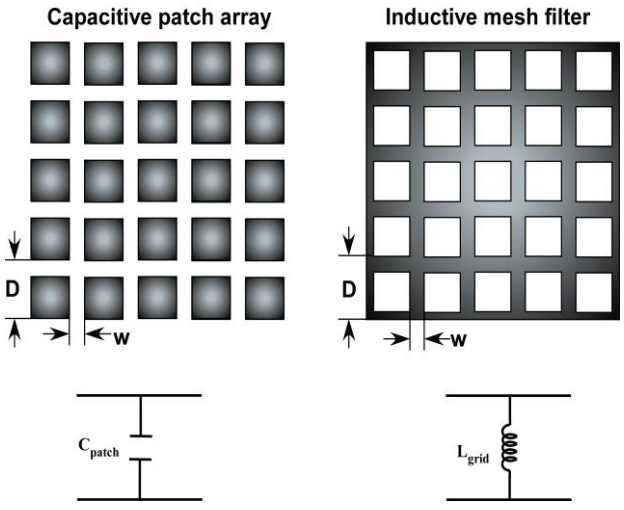

Fig. 2. Bi-dimensional sketch of non-resonant capacitive and inductive FSS filters with their lumped model.

The agreement between the approximated and full-wave results are good if the FSS periodicity is smaller than an half-wavelength. In [66], [67] the formulas for an array of Jerusalem crosses are also proposed, but they are sufficiently accurate only up to the first resonance of the Jcross.

B. First order retrieving method

The simple circuit model presented in the previous section can be improved by adding additional lumped components which allow to follow the FSS response even in the second zone; i.e., the resonant one. A simple LC circuit can fit the frequency response of a capacitive frequency selective surface, whereas, a shunt LC connection replaces the LC series for an inductive FSS. In absence of losses, the FSS impedance is purely imaginary and it is represented by two lumped parameters. Losses can be introduced by adding a series resistance in the equivalent circuit [68]-[70].

In order to compute FSS reactance, the knowledge of the current density on the FSS element is necessary even for the zero order approximation. Alternatively, a retrieving approach which starts from on the determination of the complex reflection coefficient through a preliminary full-wave simulation can be employed [58], [71]-[73]. Then, according to classical transmission line theory, it is possible to obtain the impedance of the freestanding FSS as follows:

$$Z_{FSS} = -\frac{Z_0^2\left(1+\Gamma_{in}\right)}{2Z_0\Gamma_{in}}, \quad (4)$$

where Γ_{in} is the reflection coefficient of the periodic structure calculated at the FSS position and Z_0 is the free space impedance. Once computed the FSS impedance at two frequency points, it is possible to calculate the values of the capacitance and the inductance approximating the actual impedance by solving a two equations system [58]. Even if the inversion procedure is quick, it is unstable with respect to the chosen inversion frequency points ω_1 and ω_2, leading to some inaccuracies in the calculation of L and C values. A more reliable procedure starts from the calculation of the null of the FSS impedance and then computes the inductance by an iterative procedure which minimizes the Euclidean distance between the MoM and the LC series impedance, while imposing $C = 1/\omega_{zero}^2 L$. If the frequency selective surface is embedded within dielectric layers, additional transmission lines representing the dielectric layers need to be considered in retrieving L and C parameters. Figure 3 reports, for instance, the model of an FSS embedded within two dielectric layers. The reflection coefficient Γ_{in} used in (4) is determined from the

reflection coefficient Γ_d obtained with a full-wave simulation. The additional quantities are defined in Fig. 1. After the calculation of the load impedance Z_L by using classical transmission line formulas, it is sufficient to solve a simple parallel circuit to extract the FSS impedance as shown above.

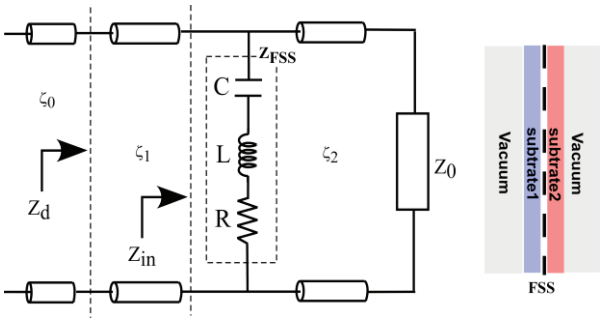

Fig. 3. Transmission line model for the analysis of an embedded FSS.

The equivalent circuit parameters are obtained for a particular FSS configuration but several degrees of freedom; e.g., repetition period of the unit cell, the angle of incidence of the incoming wave, influence the values of the equivalent inductance and capacitance. If these corrections are understood and modeled, the capacitances and inductances, preemptively obtained at normal incidence and stored in a database of shapes, can be used for computing the response of generic FSS configurations with no additional computation effort. Let us now briefly analyze separately the effect of these degree of freedom.

Cell periodicity

If all FSS element geometrical dimensions are simply rescaled with a certain scaling factor, a shift of the resonance frequencies is obtained. Starting from a given periodicity (e.g.: 10 mm), the frequency behavior of the scaled FSS can be obtained by rescaling all the inductance and capacitance values. Clearly, this stretch of the unit cell leads to the modification of the elements lengths as well. For this reason it is more convenient to think FSS element dimensions not as an absolute value but referred to the element periodicity.

Dielectric effects

The resonant frequency of an FSS in presence of a thick dielectric substrates on both sides is reduced by a factor equal to $\sqrt{\varepsilon_r}$, and by a factor $\sqrt{(\varepsilon_r+1)/2}$ when the dielectric is present only on one side of the FSS [51]. However, fixing the relative permittivity of the substrate, the decrease of its thickness leads to a gradual shift of the FSS resonance towards higher frequencies.

The presence of thin dielectric substrates involves a relevant number of Floquet modes [62], and given the complexity of the problem, a closed formula which relates the capacitance to the dielectric thickness and permittivity is hard to find. A good solution can be the derivation of a simple interpolating formula which exactly matches the variation of the effective permittivity as a function of the dielectric thickness. To this aim, the variation of capacitance as a function of thickness and dielectric constant of the substrate is analyzed for a patch array embedded within two dielectric substrates. The optimal capacitance values obtained with the retrieving procedure are normalized to the freestanding values to obtain a thickness dependent effective permittivity. An expression that fits very well, the effective permittivity reads [58]:

$$\varepsilon_{eff} = \varepsilon_r^{av} + \left(\varepsilon_r^{av} - 1\right)\left[\frac{-1}{\exp^N(x)}\right], \qquad (5)$$

where $x=10*d/D$, $\varepsilon_r^{av} = \left(d_1\varepsilon_{r1} + d_2\varepsilon_{r2}\right)/\left(d_1 + d_2\right)$ and N is an exponential factor that takes into account the slope of the curve. This parameter can vary for different cell shapes depending on the unit cell filling factor [58]. The effective permittivity as a function of the dielectric thickness obtained by using MoM simulations and the interpolating relation is shown in Fig. 4.

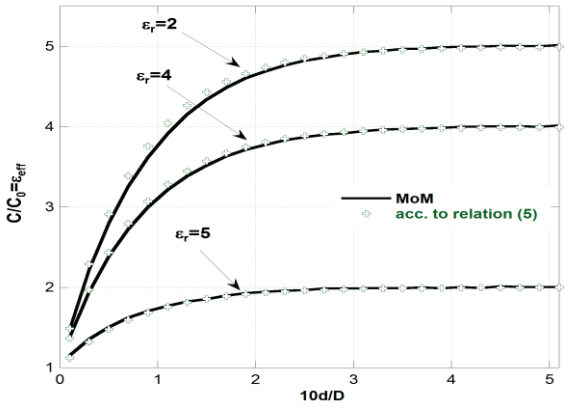

Fig. 4. Effective permittivity as a function of substrate thickness computed by iterative MoM simulations. Parameters are: D=10 mm, w=2.5 mm. The fitting of numerical values has been obtained by means of the formula (5).

Incidence angle

When an oblique electromagnetic wave strikes the FSS, the impedance of the periodic structure should be expressed in a matrix form. The mutual terms due to the coupling between the modes and the dependence on azimuthal angle ϕ, can be considered negligible for symmetric unit cells. In this case, the expression of the FSS impedance for oblique incidence becomes a two terms matrix valid for TE and TM polarizations. In order to get some insight in the angular variation of the FSS impedance, the expressions derived for patch arrays by using the averaged approach [62] can help. These expressions include the first order tangential derivative, and therefore are valid for normal and oblique incidence when the grid is reasonably homogeneous (D<λ/2). According to this formulation, the patch array capacitance for TE polarization is angle dependent [51]. The same expression can be used as an interpolating function for all elements by just replacing the number *2* with a parameter α, which in our case, would depend from the chosen element:

$$C_{TE}^{\vartheta} = C_{TE}^{0}\left(1-\frac{k_0^2}{k_{eff}^2}\frac{\sin^2(\vartheta)}{\alpha}\right), \qquad (6)$$

where C_{TE}^{0} is the capacitance computed at normal incidence, and the other quantities have been already defined.

The dependence of the FSS capacitance on the incident angle is analyzed by the MoM iterative procedure for different elements (Fig. 5). The variations of patch and ring capacitance are in agreement with the relation (6) when the parameter α is suitably chosen. The angular dependence of the TE capacitance is weak in the case of a cross element. The angular dependence of the TM capacitance can be neglected for capacitive elements.

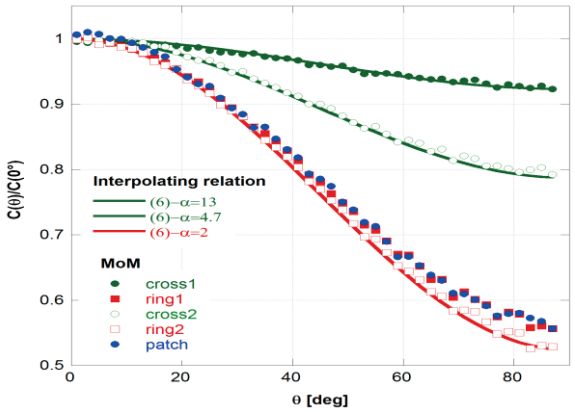

Fig. 5. Dependence of lumped capacitance on the incidence angle for different shapes.

C. Multi-mode approach

The generalized analysis presented in Section III is valid in the resonance region of the FSS, since frequency response of FSSs above the visible range involve non-linear behaviors due to the onset of higher order Floquet modes. In this region, the energy is not reflected or transmitted only in the direction stated by the Snell law, but also in other directions according to Rayleigh theory [5].

In order to describe the behavior of frequency selective surfaces in the frequency region between resonant zone and the grating lobe propagation zone as well as after the propagation of the grating lobes, a number of additional elements are necessary in the circuit model. To this purpose, two additional impedances can be connected in series with the lumped circuit comprising inductances and capacitances to take into account resonant phenomena due to the lattice [63]. The improved circuit model is reported in Fig. 6. The two impedances, which take into account the TE and TM high-order Floquet modes, read [63]:

$$Z_L(\omega) = \sum_{h=1}^{N_{TE}} A_h^{TE} Z_{TE,h}^{in}(\omega), \qquad (7)$$

$$Z_C(\omega) = \sum_{g=1}^{N_{TM}} A_g^{TM} Z_{TM,g}^{in}(\omega), \quad (8)$$

where A_h and A_g account the degree of excitation of the harmonics, the indices h and g are referred to a particular couple of *(m,n)* pair. The excitation factors, in general, depend on the frequency, but if the current on the FSS element does not significantly vary, they can be reasonably hypothesized frequency independent [63]. This hypothesis is verified when the element does not resonate in the second FSS region of Fig. 1, that is, the size of the element is much smaller than FSS periodicity. Z_{TE}^{in} and Z_{TM}^{in} represent the shunt connection between the impedances seen from the left and from the right of the FSS [74]:

$$Z_{TE,h}^{in}(\omega) = \left(\frac{1}{Z_{v,TE,h}^{left}} + \frac{1}{Z_{v,TE,h}^{right}} \right), \quad (9)$$

$$Z_{TM,g}^{in}(\omega) = \left(\frac{1}{Z_{v,TM,g}^{left}} + \frac{1}{Z_{v,TM,g}^{right}} \right). \quad (10)$$

Left and right impedances are derived, for any considered mode *(m,n)*, by using the conventional transmission line relation recursively for every substrate:

$$Z_{v,c}^{TE/TM,right/left,h/g} = Z_c^{TE,TM} \frac{\left[Z_{v,c-1}^{TE,TM} + Z_c^{TE,TM} \tan\left(k_{z,c} d_c\right) \right]}{\left[Z_c^{TE,TM} + Z_{v,c-1}^{TE,TM} \tan\left(k_{z,c} d_c\right) \right]}. \quad (11)$$

In (11) c stands for the c^{th} dielectric layer. $Z_c^{TE,TM}$ represents the modal characteristic impedance of every dielectric slab and is calculated as follows:

$$Z_{c,mn}^{TE}(\omega) = \frac{\omega \mu_0}{k_{z,mn}}, \quad (12)$$

$$Z_{c,mn}^{TM}(\omega) = \frac{k_{z,mn}}{\omega \varepsilon_0 \varepsilon_r}, \quad (13)$$

where $k_{z,mn} = \sqrt{\varepsilon_r k_0^2 - k_x^2 - k_y^2}$ is the normal component of the wavenumber. The transverse wavenumbers are:

TE polarization

$$k_{x,m} = k_0 \sin(\vartheta) + 2m\pi / D_x;\ k_{y,n} = 2n\pi / D_y$$

TM polarization

$$k_{x,m} = 2m\pi / D_x;\ k_{y,n} = k_0 \sin(\vartheta) + 2n\pi / D_y \ . \quad (14)$$

The values of the excitation coefficients and the L and C parameters can be calculated after a run of a full-wave simulation in a sufficient number of frequency points. In [63], it is suggested to choose a couple of frequency points in the low frequency range and one frequency point just before the onset of every considered high-order mode, but when the number of harmonic increases the procedure is not always stable. The introduction of many high-order modes allows to describe a highly non-linear frequency response of FSSs within the grating lobe zone provided that the element does not resonate. As the element becomes resonant within the zero-order harmonic frequency range, the current distribution cannot be anymore assumed as frequency independent. As a consequence, the harmonic excitation coefficients A in (7) and (8), may become frequency dependent leading to a reduction of accuracy of the method within the grating lobe zone. As remarked in [63], the multi-mode approach is a matching procedure mainly aimed to understand the physical mechanisms which lead to nonlinearities in the frequency response of FSSs.

It has been finally pointed out, that the described multi-mode approach is also helpful to improve the accuracy of the first order retrieving method between the resonant zone up to the propagation of the first grating lobe. To this aim, it is sufficient to include the first high order mode ($TE_{-1,0}$ for TE excitation, and $TM_{0,-1}$ for TM excitation) by computing its excitation coefficient.

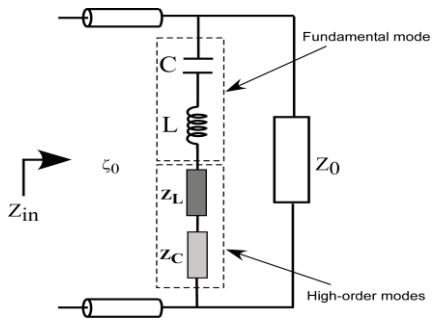

Fig. 6. Equivalent circuit of a single resonant FSS with high-order impedances.

IV. CALCULATION OF THE FREQUENCY RESPONSE OF A GENERIC FSS SYSTEM

Once derived the equivalent circuit parameters, the approximate reflection and transmission coefficients (s_{11}, s_{21}) of the FSS are

computed by using conventional transmission line theory [76]:

$$s_{11} = \frac{AZ_0 + B - CZ_0^2 - DZ_0}{AZ_0 + B + CZ_0^2 + DZ_0}, \quad (15)$$

$$s_{21} = \frac{2Z_0}{AZ_0 + B + CZ_0^2 + DZ_0}, \quad (16)$$

where A, B, C, D represents the terms of the ABCD matrix of the system comprising the FSS and a generic number N of dielectrics:

$$\begin{bmatrix} A & B \\ C & D \end{bmatrix} = [M_1] \cdot \ldots \cdot [M_n] \cdot [M_{FSS}] \cdot [M_{n+1}] \cdot \ldots \cdot [M_N]. \quad (17)$$

In equation (17), the subscript n stands for the nth dielectric substrate and M represents the scattering matrix of every layer:

$$[M_n] = \begin{bmatrix} \cos(k_{zn} d_n) & jZ_n \sin(k_{zn} d_n) \\ j\dfrac{\sin(k_{zn} d_n)}{Z_n} & \cos(k_{zn} d_n) \end{bmatrix} \quad (18)$$

$$[M_{FSS}] = \begin{bmatrix} 1 & 0 \\ 1/Z_{FSS} & 1 \end{bmatrix},$$

where Z_{FSS} is the approximate FSS impedance computed with the retrieved LC parameters, $Z_n^{TE} = (\omega \mu_r \mu_0)/k_{zn}$ and $Z_n^{TM} = k_{zn}/(\omega \varepsilon_r \varepsilon_0)$ are the characteristic impedances of the slab for TE and TM polarization, $k_{zn} = \sqrt{\varepsilon_r k_0^2 - k_t^2}$ is the normal component of the wavenumber, $k_t = k_0 \sin(\vartheta)$ is the transverse component of the wavenumber with ϑ representing the incidence angle of the incoming wave with respect to the normal and k_0 the free space propagation constant. The quantities ε_0, ε_r, μ_0, μ_r represent the free space and the relative dielectric permittivity and magnetic permeability. Since the FSS is a passive reciprocal system, the transmission coefficient of the structure is identical independently of the incidence side. If the analyzed configuration is symmetrical (same dielectrics on both side of the FSS) also, the reflection coefficients computed on the two sides of the FSS coincide (symmetric scattering matrix).

V. FSS ELEMENTS AND RESULTS

The choice of the suitable element is of outmost importance in the design of a frequency selective surface. An almost infinite set of geometries can be adopted as unit cell of a periodic screen. Some of these geometries are more popular than others and are also simple to control. We propose in Table 1 a classification of the most popular geometries on the basis of resonant properties and equivalent circuits. The number of lumped elements is directly proportional to the number of resonances. It can be demonstrated that the expression of the FSS reactance satisfies the Foster theorem [75], that is, it possesses the same pole-zero analytical properties as a passive LC network.

Table 1: Classification of FSS elements on the basis of resonant properties (symbol // means shunt connection and multiplication means series connection)

Element Type	Element Shape	Equivalent Circuit
Non-resonant elements	Strip, patch, wire grid	C
Single-resonant	Loop, dipole, cross, tripole, dogbone	(LC)
Double-resonant	Double cross, double loop, Jerusalem cross, etc.	(LC)//(LC) or (LC)(L//C)
Multi-resonant (geometrical)	Concentric loops, fractal elements	(LC)//(LC)// (LC)….
Multi-resonant (current distribution)	Quadrifilar spiral, meandered dipole or loop, genetically optimized	Not physical

In the following paragraphs some numerical results about some popular FSS elements are shown with the aim to demonstrate the validity regions of the presented equivalent circuits.

Non-resonant elements-patch arrays

The first analyzed configuration is a simple patch array. For this element, it is possible to compare the first-order retrieving model with the analytical averaged model. Even if a purely analytical approach should not be compared with a semi-analytical one, this comparison serves to show that the inclusion of the inductance in the equivalent circuit allows going beyond the limits

of effective grid parameters. The patch is characterized by a periodicity of 10 mm, which leads to the onset of grating lobes for normal incidence at 30 GHz. Figure 7 reports the reflection coefficients obtained by employing approximate impedances for two different values of the patch gap. For large gaps, the retrieving method agrees very well with the MoM code up to the propagation of the grating lobes, while the averaged model loses its validity when the cell repetition period exceeds an half wavelength. For small gaps, the averaged model is instead applicable closer to the frequency where grating lobes emerge. The capacitances obtained by using averaged relations and by using the retrieving approach are summarized in Table 2. The values computed by the retrieving approach are systematically lower than those computed by using averaged relations, since the employed circuit model considers also the inductive component of the impedance.

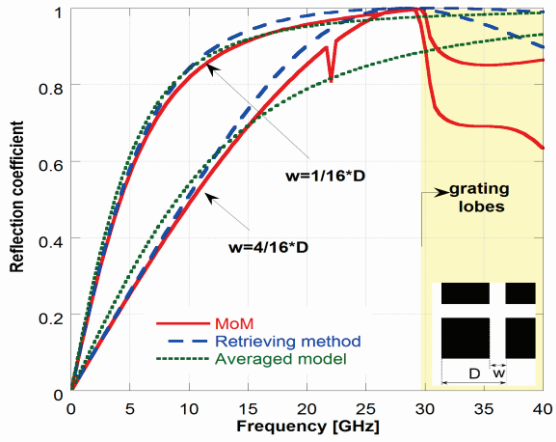

Fig. 7. Reflection coefficients obtained with different models. Parameters: D=10 mm and different w.

Table 2: Capacitance and inductance values computed by using averaged relations and by using the retrieving method (patch array with periodicity, D=10 mm)

	C_0 Averaged [fF]	C_0 Retrieved [fF]	L_0 Retrieved [nH]
w=12/16*D	54.12	43.76	0.729
w=14/16*D	90.28	81.04	0.352
w=15/16*D	130.9	117.35	0.24

Single-resonant elements

A couple of popular resonant FSS elements are the loop and the cross type. The resonance of the loop occurs when the length approaches to one wavelength while the cross element resonates when its length equals half wavelength. Figures 8 and 9 report the impedance and the reflection coefficient for a cross shaped FSS. The approximated responses are computed both by using the retrieving method and the multimode approach. The multimode approach includes just the first high-order mode in order to limit the complexity of the equivalent circuit.

It is evident that the resonant behavior of the element is caught by the LC circuit while the effects due to the lattice (Wood's anomaly) are well approximated only by including at least one high order mode. The geometrical parameters of the simulated cross are reported in Table 3 together to the values of the lumped elements employed in the transmission line model to retrieve the FSS response. In Fig. 10, the reflection coefficient for a loop shaped FSS is also reported. Also in this case, the introduction of the first HO harmonic allows to correctly match the reflection behavior up to the onset of the grating lobes. Table 4 reports the geometrical parameter of the simulated loop element together to the values of the lumped elements employed in the circuit model to retrieve the FSS response.

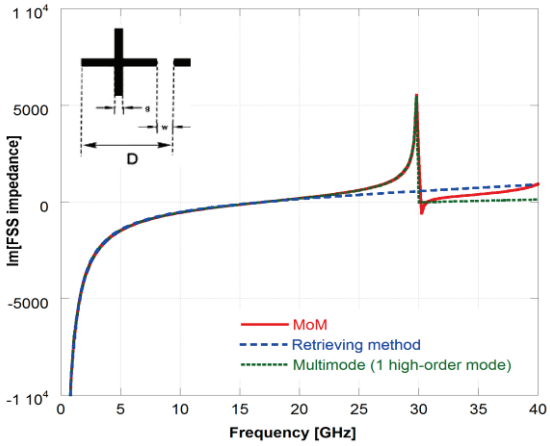

Fig. 8. Impedance of a freestanding cross FSS obtained through MoM approach, the retrieving method and the multi-mode approach with one high-order mode (TE01). Geometrical parameters: D=10 mm, w=2/16*D, g=2/16*D.

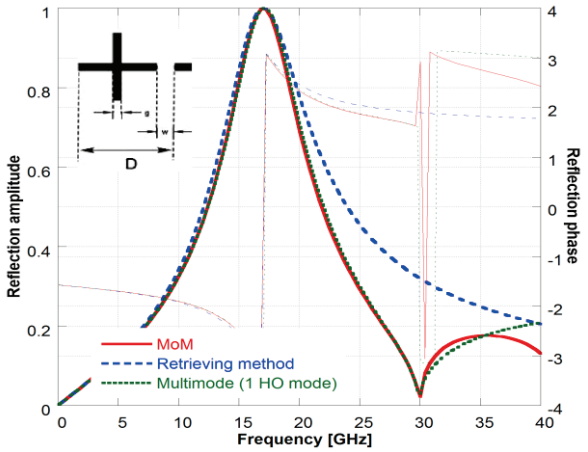

Fig. 9. Reflection coefficient of a freestanding cross FSS obtained by using MoM code, the retrieving method and the multi-mode approach including only 1 high-order mode (TE01). Geometrical parameters: D=10 mm, w=2/16*D, g=2/16*D.

Table 3: Geometrical parameters and values of the electrical parameters in the lumped circuits of the simulated cross element

Physical Parameters		Retrieving Method		Multi-mode Circuit (1 HO mode)	
D	10 mm	C_s	20.00 fF	C_s	19.91 fF
G	2/16*D	L_s	4.37 nH	L_s	1.29 nH
W	2/16*D			A_{1TE}	2.49

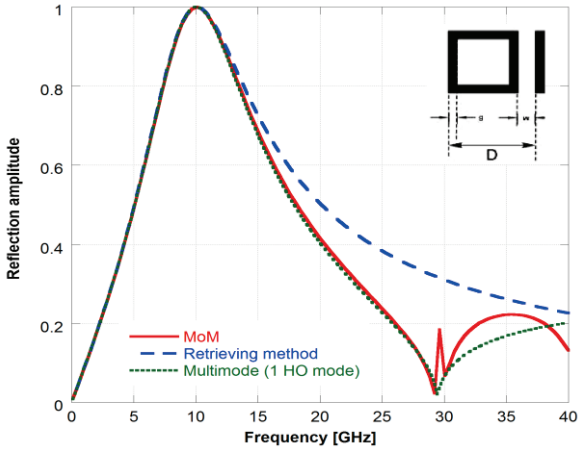

Fig. 10. Reflection coefficient of a freestanding loop shaped FSS obtained by using MoM code, the retrieving method and the multi-mode approach including only 1 high-order mode. Geometrical parameters: D=10 mm, w=2/16*D, g=1/16*D.

Table 4: Geometrical parameters and values of the electrical parameters in the lumped circuits of the simulated loop element

Physical Parameters		Retrieving Method		Multi-mode Circuit (1 HO mode)	
D	10 mm	C_s	72.34 fF	C_s	72.39 fF
g	1/16*D	L_s	3.45 nH	L_s	0.61 nH
w	2/16*D			A_{1TE}	2.67

Multi-resonant elements

There is often the necessity of employing more complex FSS elements in the design of narrow band, multi-band filters or even in multi-resonant High-Impedance Surfaces (HIS) [77], [78]. Some FSS elements can generate a double resonant, or more in general, a multi-resonant behavior in the zero-order Floquet propagating zone. These structures can be analyzed by introducing additional lumped elements in the resonant circuit. A common FSS shape is the so called Jerusalem Cross. This element is basically a cross with loading ends which enhance the capacitance value. An additional series LC circuit in parallel with the original one in the equivalent circuit is needed, since the electric field couples also with the two end-loading dipoles. A layout of the geometry of the double resonant unit cell and its corresponding equivalent circuit is shown in Fig. 11.

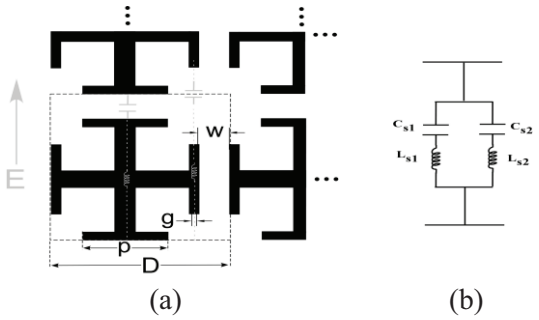

Fig. 11. Jerusalem cross element: (a) with its equivalent circuit and cross-frame element and (b) with its equivalent circuit.

The impedance of the circuit reads:

$$Z_{LC//LC} = \frac{\left(1-\omega^2 L_{s1}C_{s1}\right)\left(1-\omega^2 L_{s2}C_{s2}\right)}{j\omega\left[C_{s1}+C_{s2}-\omega^2 C_{s1}C_{s2}\left(L_{s1}+L_{s2}\right)\right]}. \quad (19)$$

The values of the unknown capacitance and inductances can be computed by solving by running an iterative matching procedure. The

procedure starts from the computation of the three resonance frequencies ω_{z1}, ω_{z2} and ω_{p2}, by detecting the nulls of the derivative function of the actual FSS impedance. The following relations between the lumped components of the LC//LC circuit hold:

$$C_{s1} = \frac{1}{L_{s1}\omega_{z_1}^2};\ C_{s2} = \frac{1}{L_{s2}\omega_{z_1}^2};$$
$$L_{s2} = \frac{\left(\frac{\omega_{p2}^2}{\omega_{z2}^2}\right)L_{s1}C_{s1} - \left(\frac{1}{\omega_{z2}^2}\right)}{C_{s1}\left(1 - \frac{\omega_{p2}^2}{\omega_{z2}^2}\right)}. \quad (20)$$

The value of the inductance L_{s1} is obtained by an iterative procedure that minimizes the Euclidean distance between the impedance computed by the MoM approach and the one obtained by the equivalent circuit model. The first pole ω_{p1} falls at $\omega=0$ since the FSS is capacitive. Figure 12 shows the comparison between the reflection coefficients obtained by a MoM analysis and by the circuital approach for the two analyzed FSS configuration. The lumped components are summarized in Table 5, where the values of the geometrical parameters are also specified. The value of the capacitance C_{s1} is higher than that of the simple cross, since the end loading improves the capacitive coupling between the neighboring crosses. The additional capacitor, due to the capacitive effect introduced by the two end loading strips aligned with the electric field is lower than the main effect, due to the central cross as expected.

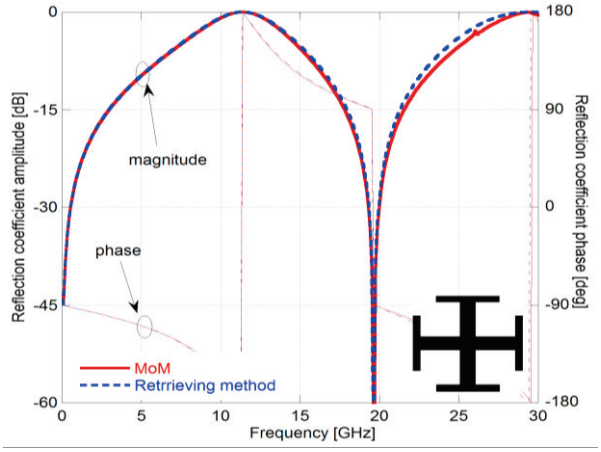

Fig. 12. Reflection coefficient of a freestanding Jerusalem cross array obtained by a periodic MoM approach and by the retrieving method.

Table 5: Lumped parameters of the simulated Jcross (the geometrical parameters are: D=10 mm, w=D/8, g=D/16, p=3/8D)

Jerusalem Cross Array			
C_{s1}	37.93 fF	C_{s2}	10.70 fF
L_{s1}	5.15 nH	L_{s2}	2.71 nH

The surface current on the Jerusalem cross and the electric field distribution on the same plane are reported at the two resonances with unitary reflection (i.e.: 11 GHz and 29 GHz) in Fig. 13. As it is evident from the color plot, the central cross is mostly excited in correspondence of the former resonance, while the end loading dipole represented by the second LC series circuit determines the position of the latter resonance (its length is equal to an half wavelength in correspondence of the second unitary reflection resonance). FSS elements characterized by a higher number of resonances within the fundamental Floquet harmonic zone can still be modeled by extending the aforementioned equivalent circuits to n^{th} order resonant circuits [78].

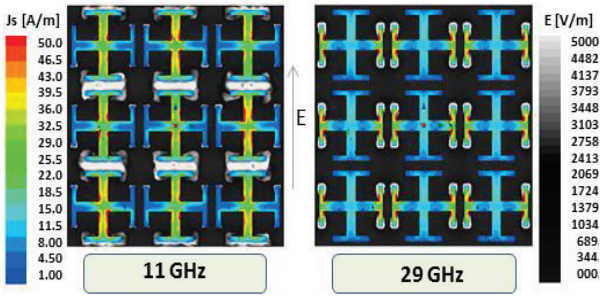

Fig. 13. Surface current and electric field distribution on the plane of the Jerusalem cross array at the two reflection resonances.

A multi-resonant element useful for understanding the limitations of the equivalent circuit approach is the spiral cross array. The matching of the reflection coefficient of the investigated spiral structure can be obtained by using the same equivalent circuit of Jcross as reported in Fig. 14. However, in this case the equivalent circuit does not catch the physical behavior of the structure. Indeed, differently from the previous multi-resonant element, where the resonances were due to the element geometry, this

element resonates because of the high-order modes of the current distribution. As it is evident from Fig. 15, the fundamental resonance occurs when the length of the spiral approaches at half wavelength, while the second resonance occurs when the length of the arms is equal to 3/2λ. Other more complex and more compact element configurations are also possible [79], [80] and their behavior can still be matched by using a pole-zero matching procedure [75].

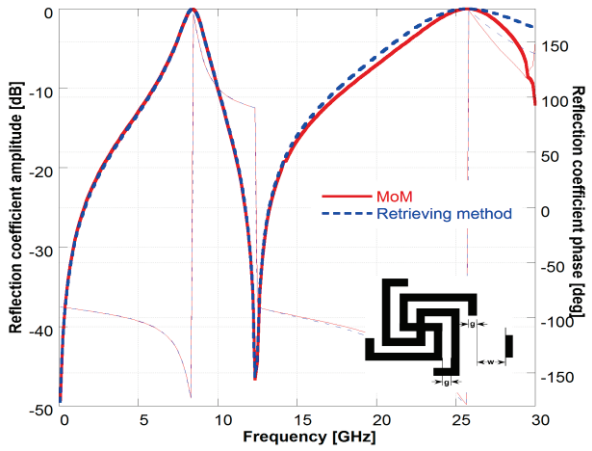

Fig. 14. Reflection coefficient of a freestanding spiral cross array obtained by MoM approach and by the retrieving method. The geometrical parameters are: D=10 mm, w=3/16D, g=D/16.

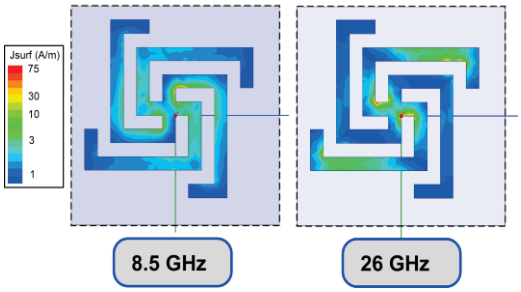

Fig. 15. Surface current on the plane of the spiral cross array at the two reflection resonances.

VI. DISCUSSION ON LUMPED ELEMENTS VALUES

Simple electrostatic relationships can be exploited to qualitatively understand the reason why certain shapes determine specific values of capacitance and inductance. As it is well known, the static capacitance of an ideal parallel plate capacitor is directly proportional to the plate area A and inversely proportional to the plate separation d ($C = \varepsilon_0 \varepsilon_r A/d$). The capacitance value of the cross element is the lowest one, since the parallel plate capacitor formed by the two adjacent crosses has a small area. For the same reason, the patch capacitance is comparable than the loop one.

In Fig. 16, the capacitance values for different unit cell elements are reported as a function of the element over periodicity. It is clear the capacitive coupling increases exponentially by reducing the gap between adjacent elements. The inductance values can be explained by resorting to the expression of the inductance of two parallel wires with length l, radius a and distance d ($L = l/\pi \ln(d/a)$). As the distance between the parallel wires decreases, the inductance decreases as well. In the case of the patch element, we can infer that the inductance value is very low because the plate is very large and in the previous formula corresponds, unwrapping the wire, to enhance the value of the wire radius. Cross and loop elements are characterized by higher inductances because of the narrow strips composing the single element. By observing the calculated optimal values of the inductances in Tables 3 and 4, it is evident the inductance values drop as the first TE high order mode is included in the multi-mode model. This is due to the fact that the impedance of the first TE harmonic is inductive. As a consequence, the inductive component of the element is now shared between the inductor and the first TE harmonic.

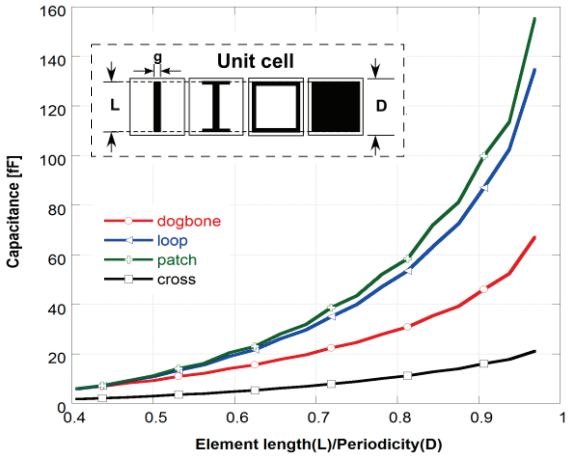

Fig. 16. Capacitance values of 4 different elements as a function of the element size with respect to the lattice periodicity. The element width (g) is fixed to D/16.

VII. CONCLUSION

A comprehensive overview of FSS circuit modeling has been presented. Different models based on fully analytical or semi-analytical formulations are described with the aim to clarify their range of validity and their accuracy. Fully analytical models based on averaged expressions are accurate for dense periodic arrays (quasi-static region), while a simple semi-analytical approach can be employed also in the resonant region of FSSs. The latter approach can be applied to generic FSS elements and it can be generalized with simple relations. Finally, an efficient multi-mode approach which allows to match the complex response of the FSS screens within non-linear grating lobes region has also been discussed.

REFERENCES

[1] D. Rittenhouse, "An optical problem, proposed by mr. hopkinson, and solved by mr. Rittenhouse," *Trans. Amer. Phil. SOC.*, vol. 2, pp. 201-206, 1786.

[2] E. G. Loewen and E. Popov, "Diffraction gratings and applications," *CRC Press*, 1997.

[3] R. W. Wood, "On a remarkable case of uneven distribution of light in a diffraction grating spectrum," *Philos. Mag.*, vol. 4, pp. 396-402, 1902.

[4] L. Rayleigh, "Note on the remarkable case of diffraction spectra described by prof. wood," *Philos. Mag*., vol. 14, pp. 60-65, 1907.

[5] L. Rayleigh, "On the dynamical theory of gratings," *Proceedings of the Royal Society of London. Series A, Containing Papers of a Mathematical and Physical Character*, 79 (532), pp. 399-416, 1907.

[6] U. Fano, "The theory of anomalous diffraction gratings and of quasi-stationary waves on metallic surfaces (sommerfeld's waves)," *J. Opt. Soc. Am*., vol. 31, pp. 213-222, March 1941.

[7] A. Hessel and A. A. Oliner, "A new theory of wood's anomalies on optical gratings," *Applied Optics*, 4.10, 1275-1297, 1965.

[8] G. Marconi and C. S. Franklin, "Reflector for use in wireless telegraphy and telephony," *US Patent 1,301,473*, April 1919.

[9] G. von Trentini, "Partially reflecting sheet arrays," *IRE Trans. Antennas Propagation*, vol. AP-4, pp. 666-671, 1956.

[10] N. Marcuvitz (ed.), "Waveguide handbook," IEE Electromagnetic Waves Series 21, *McGraw-Hill*, New York, 1951.

[11] W. Rotman and A. A. Oliner, "Periodic structures in trough waveguide," *IRE Trans. on Microwave Theory and Tech.*, vol. 7, no. 1, pp. 134,142, January 1959.

[12] L. Goldstone and A. A. Oliner, "Leaky-wave antennas I: rectangular waveguides," *IRE Trans. on Antennas and Propag.*, vol. 7, no. 4, pp. 307,319, October 1959.

[13] D. R. Jackson and N. G. Alexópoulos, "Gain enhancement methods for printed circuit antennas," *IEEE Trans. Antennas Propag.*, vol. 33, pp. 976-987, September 1985.

[14] D. R. Jackson and A. A. Oliner, "A leaky-wave analysis of the high gain printed antenna configuration," *IEEE Trans. Antennas Propag.*, vol. 36, no. 7, pp. 905-910, 1988.

[15] T. Zhao, D. R. Jackson, J. T. Williams, H. D. Yang, and A. A. Oliner, "2-D periodic leaky-wave antennas-part I: metal patch design," *IEEE Trans. Antennas Propag.*, vol. 53, no. 11, pp. 3505-3514, 2005.

[16] G. Lovat, P. Burghignoli, and D. R. Jackson, "Fundamental properties and optimization of broadside radiation from uniform leaky-wave antennas," *IEEE Trans. Antennas Propag.*, vol. 54, pp. 1442-1452, 2006.

[17] V. Agrawal and W. Imbriale, "Design of a dichroic cassegrain subreflector," *IEEE Trans. on Antennas and Propag.*, vol. 27, no. 4, pp. 466-473, July 1979.

[18] T. K. Wu, "Four-band frequency selective surface with double-square-loop patch elements," *IEEE Trans. on Antennas and Propag.*, vol. 42, no. 12, 1994.

[19] B. A. Munk, "Frequency selective surfaces-theory and design," *John Wiley & Sons*, New York, 2000.

[20] T. K. Wu, "Frequency selective surface and grid array," New York, *John Wiley & Sons, Inc*., 1995.

[21] F. Costa and A. Monorchio, "A frequency selective radome with wideband absorbing properties," *IEEE Trans. on Antennas and Propag.*, vol. 60, no. 6, pp. 2740-2747, 2012.

[22] D. R. Jackson, P. Burghignoli, G. Lovat, F. Capolino, J. Chen, D. R. Wilton, and A. A. Oliner, "The fundamental physics of directive beaming at microwave and optical frequencies and the role of leaky waves," *Proc. of the IEEE*, vol. 99, no. 10, pp. 1780-1805, 2011.

[23] F. Costa, O. Luukkonen, C. R. Simovski, A. Monorchio, S. A. Tretyakov, and P. De Maagt, "TE surface wave resonances on high-impedance surface based antennas: analysis and modeling," *IEEE Trans. on Antennas and Propag.*, vol. 59, no. 10, pp. 3588-3596, October 2011.

[24] S. Genovesi, F. Costa, A. Monorchio, "Wideband Radar Cross Section Reduction of Slot Antennas Arrays" *IEEE Trans. on Antennas and Propag.*, vol. 62, no. 1, pp. 163-173, January 2014.

[25] N. Gagnon, A. Petosa, and D. A. McNamara, "Research and development on phase-shifting

surfaces (PSSs)," *IEEE Antennas and Propagation Magazine*, vol. 55, no. 2, pp. 29-48, April 2013.

[26] J. Huang, "Reflectarray antenna," *John Wiley & Sons, Inc*., 2007.

[27] R. Lech, M. Mazur, and J. Mazur, "Analysis and design of a polarizer rotator system," *IEEE Trans. on Antennas and Propag*., vol. 56, no. 3, pp. 844-847, March 2008.

[28] F. Costa, C. Amabile, A. Monorchio, and E. Prati, "Waveguide dielectric permittivity measurement technique based on resonant FSS filters," *IEEE Microwave and Wireless Comp. Letters*, vol. 21, no. 5, pp. 273-275, May 2011.

[29] M. Philippakis, et al., "Application of FSS structures to selectively control the propagation of signals into and out of buildings," *Ofcom Ref. AY4464A*, 2004.

[30] F. Costa, A. Monorchio, and G. Manara, "Analysis and design of ultra thin electromagnetic absorbers comprising resistively loaded high impedance surfaces," *IEEE Trans. on Antennas and Propag*., vol. 58, no. 5, pp. 1551-1558, 2010.

[31] J. B. Pendry and D. R. Smith, "The quest for the superlens," *Sci. Amer.*, vol. 295, no. 1, pp. 60-67, July 2006.

[32] T. Maier and H. Bruckl, "Wavelength-tunable microbolometers with metamaterial absorbers," *Optics Letters*, vol. 34 (19), p. 3012, 2009.

[33] S. A. Kuznetsov, A. G. Paulish, A. V. Gelfand, P. A. Lazorskiy, and V. N. Fedorinin, "Bolometric THz-to-IR converter for terahertz imaging," *Appl. Phys. Lett*., vol. 99, 023501, 2011.

[34] H. T. Chen, W. J. Padilla, M. J. Cich, A. K. Azad, R. D. Averitt, and A. J. Taylor, "A metamaterial solid state terahertz phase modulator," *Nature Photonics*, vol. 3, 148-151, 2009.

[35] E. Rephaeli and S. Fan, "Absorber and emitter for solar thermophotovoltaic systems to achieve efficiency exceeding the shockley-queisser limit," *Opt. Express*, 17, 15, 145-159, 2009.

[36] Liu, T. Tyler, T. Starr, A. F. Starr, N. M. Jokerst, and W. J. Padilla, "Taming the blackbody with infrared metamaterials as selective thermal emitters," *Phys. Rev. Lett*., 107(4), p. 045901, 2011.

[37] C. C. Chen, "Transmission through a conductive screen perforated periodically with apertures," *IEEE Trans. Microwave Theory & Tech.*, vol. 18, no. 9, pp. 627-632, 1970.

[38] R. Mittra, C. H. Chan, and T. Cwik, "Techniques for analyzing frequency selective surfaces, a review," *Proc. of the IEEE*, vol. 76, no. 12, pp. 1593-1615, 1988.

[39] R. Orta, R. Tascone, and R. Zich, "A unified formulation for the analysis of general frequency selective surfaces," *Electromagnetics*, vol. 5, no. 4, pp. 307-329, 1985.

[40] M. Bozzi and L. Perregrini, "Efficient analysis of thin conductive screens perforated periodically with arbitrarily shaped apertures," *Electronics Letters*, vol. 35, no. 13, pp. 1085-1087, June 1999.

[41] G. G. MacFarlane, "Surface impedance of an infinite wire grid, at oblique angles of incidence," *J. IEE*, vol. 93 (III E), pp. 1523-1527, December 1946.

[42] W. Wessel, "On the passage of electromagnetic waves through a wire grid," *Hochfrequenztechnik*, vol. 54, pp. 62-69, January 1939.

[43] R. Hornejäger, "Electromagnetic properties of wire grids," *Ann. der Phys*ik, vol. 4, pp. 25-35, January 1948.

[44] G. von Trentini, "Gratings as circuit elements of electric waves in space," *Zeit. angew. Phys*., vol. 5, pp. 221-231, June 1953.

[45] J. R. Wait, "The impedance of wire grid parallel to a dielectric interface," *IRE Trans. Microwave Theory Tech.*, vol. MTT-5, no. 2, pp. 99-102, April 1957.

[46] J. Young and J. R. Wait, "Note on the impedance of a wire grid parallel to a homogeneous interface," *IEEE Trans. Microwave Theory Tech.*, vol. 37, no. 7, pp. 1136-1138, July 1989.

[47] R. Ulrich, K. F. Renk, and L. Genzel, "Tunable submillimeter interferometers of the fabry-perot type," *IEEE Trans. Microwave Theory Tech.*, vol. 11, no. 5, pp. 363-371, 1963.

[48] S. W. Lee, G. Zarrillo, and C. L. Law, "Simple formulas for transmission through periodic metal grids or plates," *IEEE Trans. Antennas Propag.*, vol. AP-30, no. 5, pp. 904-909, 1982.

[49] M. I. Kontorovich, V. Y. Petrunkin, N. A. Yesepkina, and M. I. Astrakhan, "The coefficient of reflection of a plane electromagnetic wave from a plane wire mesh," *Radio Eng. Electron Phys.*, no. 7, pp. 222-231, 1962.

[50] M. I. Astrakhan, "Averaged boundary conditions on the surface of a lattice with rectangular cells," *Radio Eng. Electron Phys.*, no. 9, pp. 1239-1241, 1964.

[51] O. Luukkonen, C. Simovski, G. Granet, G. Goussetis, D. Lioubtchenko, A. V. Räisänen, and S. A. Tretyakov, "Simple and accurate analytical model of planar grids and high-impedance surfaces comprising metal strips or patches," *IEEE Trans. on Antennas and Propag.*, vol. 56, no. 6, pp. 1624-1632, 2008.

[52] V. V. Yatsenko, S. A. Tretyakov, S. I. Maslovski, and A. A. Sochava, "Higher order impedance boundary conditions for sparse wire grids," *IEEE Trans. Antennas Propag.*, vol. 48, no. 5, pp. 720-

727, 2000.

[53] R. J. Langley and A. J. Drinkwater, "An improved empirical model for the Jerusalem cross," *IEE Proc. H, Microw. Optics and Antennas*, vol. 129, no. 1, pp. 1-6, 1982.

[54] R. J. Langley and E. A. Parker, "Equivalent circuit model for arrays of square loops," *Electronics Letters*, vol. 18, no. 7, pp. 294-296, April 1982.

[55] R. J. Langley and E. A. Parker, "Double square frequency selective surfaces and their equivalent circuit," *Electronics Letters*, vol. 19, no. 17, pp. 675-677, August 1983.

[56] C. K. Lee and R. J. Langley, "Equivalent-circuit models for frequency selective surfaces at oblique angles of incidence," *IEE Proc. H, Microwaves, Antennas and Propagation*, vol. 132, no. 6, pp. 395-399, October 1985.

[57] S. B. Savia and E. A. Parker, "Equivalent circuit model for superdense linear dipole FSS," *IEE Proc. H, Microwaves, Antennas and Propagation*, vol. 150, no. 1, pp. 37-42, February 2003.

[58] F. Costa, A. Monorchio, and G. Manara, "Efficient analysis of frequency selective surfaces by a simple equivalent circuit model," *IEEE Antennas and Propagation Magazine*, vol. 54, no. 4, pp. 35-48, 2012.

[59] P. Callaghan, E. A. Parker, and R. J. Langley, "Influence of supporting dielectric layers on the transmission properties of frequency selective surfaces," *IEE Proc. H, Microwaves, Antennas and Propagation*, vol. 138, no. 5, pp. 448-454, 1991.

[60] R. Dubrovka, J. Vazquez, C. Parini, and D. Moore, "Equivalent circuit method for analysis and synthesis of frequency selective surfaces," *IEE Proc. Microwaves, Antennas and Propag.*, vol. 153, no. 3, pp. 213-220, June 2006.

[61] S. Monni, G. Gerini, A. Neto, and A. G. Tijhuis, "Multi-mode equivalent networks for the design and analysis of frequency selective surfaces," *IEEE Trans. Antennas Propag.*, vol. 55, pp. 2824-2835, 2007.

[62] R. Rodriguez-Berral, F. Medina, F. Mesa, and M. Garcia-Vigueras, "Quasi-analytical modeling of transmission/reflection in strip/slit gratings loaded with dielectric slabs," *IEEE Trans. on Microwave Theory and Tech.*, vol. 60, no. 3, pp. 405-418, March 2012.

[63] M. Garcia-Vigueras, F. Mesa, F. Medina, R. Rodriguez-Berral, and J. L. Gomez-Tornero, "Simplified circuit model for arrays of metallic dipoles sandwiched between dielectric slabs under arbitrary incidence," *IEEE Trans. Antennas Propag.*, vol. 60, no. 10, pp. 4637,4649, October 2012.

[64] C. L. Holloway, E. F. Kuester, J. A. Gordon, J. O'Hara, J. Booth, and D. R. Smith, "An overview of the theory and applications of metasurfaces: the two-dimensional equivalents of metamaterials," *IEEE Antennas and Propagation Magazine*, vol. 54, no. 2, pp. 10,35, April 2012.

[65] S. Tretyakov, "Analytical modelling in applied electromagnetics," *Artech House*, Boston, 2003.

[66] A. B. Yakovlev, O. Luukkonen, C. R. Simovski, S. A. Tretyakov, S. Paulotto, P. Baccarelli, and G. W. Hanson, "Analytical modeling of surface waves on high impedance surfaces," *Metamaterials and Plasmonics: Fundamentals, Modelling, Applications NATO Science for Peace and Security Series B*, pp. 239-254, 2009.

[67] I. Andersson, "On the theory of self-resonant grids," *The Bell System Technical Journal*, vol. 55, pp. 1725-1731, 1975.

[68] J. E. Raynolds, B. A. Munk, J. B. Pryor, and R. J. Marhefka, "Ohmic loss in frequency-selective surfaces," *Journal of Applied Physics*, vol. 93, no. 9, pp. 5346-5358, May 2003.

[69] F. Costa, S. Genovesi, A. Monorchio, and G. Manara, "A circuit-based model for the interpretation of perfect metamaterial absorbers," *IEEE Trans. Antennas Propag.*, vol. 61, no. 3, pp. 1201-1209, March 2013.

[70] F. Costa and A. Monorchio, "Closed-form analysis of reflection losses of microstrip reflectarray antennas," *IEEE Trans. Antennas Propag.*, vol. 60, no. 10, pp. 4650-4660, October 2012.

[71] Y. E. Erdemli, K. Sertel, R. A. Gilbert, D. E. Wright, and J. L. Volakis, "Frequency selective surface to enhance performance of broad-band reconfigurable arrays," *IEEE Trans. Antennas Propag.*, vol. 40, no. 12, pp. 1716-1724, 2002.

[72] C. Mias, C. Tsokonas, and C. Oswald, "An investigation into the feasibility of designing frequency selective windows employing periodic structures," *Technical Report AY3922, The Nottingham Trent University*, Burton Street, Nottingham, NG1 4BU, U.K., 2002.

[73] M. Ohira, H. Deguchi, M. Tsuji, and H. Shigesawa, "Analysis of frequency-selective surfaces with arbitrarily shaped element by equivalent circuit model," *Electronics and Communications in Japan (Part II: Electronics)*, vol. 88, no. 6, pp. 9-17, June 2005.

[74] C. C. Chen, "Scattering by a two-dimensional periodic array of conducting plates," *IEEE Trans. Antennas Propag.*, AP-18, 660-665, 1970.

[75] S. Maci, M. Caiazzo, A. Cucini, and M. Casaletti, "A pole-zero mathcing method for EBG surfaces composed of a dipole FSS printed on a grounded dielectirc slab," *IEEE Trans. Antennas Propag.*, vol. 53, no. 1, pp. 70-81, January 2005.

[76] D. M. Pozar, "Microwave engineering," 2nd ed., *Toronto: John Wiley &Sons*, 1998.

[77] D. J. Kern, D. H. Werner, A. Monorchio, L. Lanuzza, and M. J. Wilhelm, "The design synthesis of multi-band artificial magnetic conductors using high impedance frequency selective surfaces," *IEEE Trans. Antennas Propag.*, vol. 53, no. 1, pp. 8-17, 2005.

[78] F. Costa, S. Genovesi, and A. Monorchio, "A chipless RFID based on multi-resonant high-impedance surfaces," *IEEE Trans. on Microwave Theory and Tech.*, vol. 61, no. 1, pp. 146-153, 2013.

[79] S. Genovesi, F. Costa, B. Cioni, V. Miceli, G. Annino, G. Gallone, G. Levita, A. Lazzeri, A. Monorchio, and G. Manara, "Miniaturized high impedance surfaces with angular stability by using zirconium tin titanate (ZST) substrates and convoluted FSS elements," *Microwave and Optical Technology Letters*, vol. 51, no. 11, pp. 2753-2758, August 2009.

[80] A. Vallecchi and A. G. Schuchinsky, "Entwined planar spirals for artificial surfaces," *IEEE Antennas and Wireless Propagation Letters*, vol. 9, pp. 994-997, 2010.

Filippo Costa was born in Pisa, Italy, on October 31, 1980. He received his M.Sc. degree in Telecommunication Engineering and his Ph.D. degree in Applied Electromagnetism from the University of Pisa, Pisa, Italy, in 2006 and 2010, respectively. From March to August 2009, he was a Visiting Researcher in the Department of Radio Science and Engineering, Helsinki University of Technology, TKK (now Aalto University), Finland. Since January 2010, he's been a Postdoctoral Researcher at the University of Pisa.

His research is focused on the analysis and modelling of Frequency Selective Surfaces and Artificial Impedance Surfaces with emphasis to their application in electromagnetic absorbing materials, leaky antennas, radomes, Radio Frequency Identification, waveguide filters and techniques for retrieving dielectric permittivity of materials. He was recipient of the Young Scientist Award of the URSI International Symposium on Electromagnetic Theory and URSI General Assembly in 2013 and 2014, respectively.

Agostino Monorchio received the Laurea degree in Electronics Engineering and his Ph.D. degree in Methods and Technologies for Environmental Monitoring from the University of Pisa, Pisa, Italy, in 1991 and 1994, respectively. He is currently an Associate Professor at the School of Engineering, University of Pisa, and Adjunct Professor at the Italian Naval Academy of Livorno. He is also an Adjunct Professor in the Department of Electrical Engineering, Penn State. He is on the Teaching Board of the Ph.D. course in "Remote Sensing" and on the council of the Ph.D. School of Engineering "Leonardo da Vinci" at the University of Pisa.

His research interests include the development of novel numerical and asymptotic methods in applied electromagnetics, both in frequency and time domains, with applications to the design of antennas, microwave systems and RCS calculation, the analysis and design of frequency-selective surfaces and novel materials, and the definition of electromagnetic scattering models from complex objects and random surfaces for remote sensing applications. He has been a reviewer for many scientific journals and he has been supervising various research projects related to Applied Electromagnetic, commissioned and supported by national companies and public institutions. Monorchio is IEEE Fellow. He has served as Associate Editor of the IEEE Antennas and Wireless Propagation Letters. He received a Summa Foundation Fellowship and a NATO Senior Fellowship.

Giuliano Manara received the Laurea (Doctor) degree in Electronics Engineering (summa cum laude) from the University of Florence, Italy, in 1979. Currently, he is a Professor at the School of Engineering of the University of Pisa, Italy. Since 1980, he has been collaborating with the Department of Electrical Engineering of the Ohio State University, Columbus, Ohio, where, in the summer and fall of 1987, he was involved in research at the ElectroScience Laboratory.

His research interests have centered mainly on the asymptotic solution of radiation and scattering problems to improve and extend the uniform geometrical theory of diffraction. In this framework, he has analyzed electromagnetic wave scattering from material bodies, with emphasis on the scattering from both isotropic and anisotropic impedance wedges. He has also been engaged in research on numerical, analytical and hybrid techniques (both in frequency and time domain), scattering from rough surfaces,

Frequency Selective Surfaces (FSS), and electromagnetic compatibility. More recently, his research has also been focused on the design of microwave antennas with application to broadband wireless networks, and on the development and testing of new microwave materials (metamaterials). Manara was elected an IEEE Fellow in 2004 for "contributions to the uniform geometrical theory of diffraction and its applications." In August 2011, he was elected Chair of the International Commission B of URSI.